Available online at www.sciencedirect.com

ScienceDirect

Journal of Sound and Vibration 307 (2007) 802–817

JOURNAL OF SOUND AND VIBRATION

www.elsevier.com/locate/jsvi

A coupled approach for damage detection of framed structures using piezoelectric signature

W. Yan[a,b], C.W. Lim[c,*], W.Q. Chen[a], J.B. Cai[a]

[a]*Department of Civil Engineering, Zhejiang University, Hangzhou 310027, China*
[b]*Department of Civil Engineering, Ningbo University, Ningbo 315211, China*
[c]*Department of Building and Construction, City University of Hong Kong, Kowloon, Hong Kong*

Received 14 September 2006; received in revised form 2 July 2007; accepted 11 July 2007
Available online 27 August 2007

Abstract

High-frequency electro-mechanical impedance (EMI) signature is very sensitive to the local incipient damages in structures. However, extensive information on the nature of damages may not be available via EMI technique in its conventional non-model-based form. On the other hand, there is also little analytical work on the vibration modes of complex structures at ultrasonic frequencies. In this paper, a coupled approach combining EMI technique and a reverberation matrix method is proposed to quantitatively correlate damages in framed structures with high-frequency signature for structural health monitoring. The structural members are modeled as Timoshenko beams for flexural motion and as the classical longitudinal rods for axial motion. The PZT wafers, which are bonded to the beams, are also treated as one-dimensional in an axial vibration. A shear lag model is adopted to simulate the interfacial bonding between PZT patches and the host beam. An analytical expression for impedance (or admittance) related to response of the coupled model of PZT patch–bonding layer–host frame system is derived for the first time. Comparison study is presented with other established methods and theories. Based on this analysis, EMI signatures are extracted to identify the damages in framed structures theoretically.

1. Introduction

Two-dimensional (2D) or three-dimensional (3D) frames have been extensively used in various engineering applications including civil infrastructures, large orbital space stations and the like [1–3]. The incipient damage assessment of these crucial structures is an important means to prevent and mitigate the secondary disaster [4]. Thus, many methods such as vibration-based approaches have been proposed to detect damages in structures [5]. However, the main limitation of these low-frequency techniques is that a relatively small number of the first few modes are not sufficient to detect minor damages in structures [6]. The electro-mechanical impedance (EMI) technique, which utilizes the impedance signature extracted from a PZT patch bonded onto the host structure in the high-frequency range (typically 10–500 kHz [7]), is able to detect minor changes in structural

*Corresponding author. Tel.: +852 2788 7285; fax: +852 2788 7612.
E-mail address: bccwlim@cityu.edu.hk (C.W. Lim).

0022-460X/$ - see front matter © 2007 Elsevier Ltd. All rights reserved.
doi:10.1016/j.jsv.2007.07.026

Nomenclature

a	half-length of PZT patch
A	cross-sectional area
d_{31}	piezoelectric constant
D_3	electric displacement
E_3	electric potential
E_p, E_s	Young's modulus of PZT patch and host structures, respectively
$\bar{E}_p$	complex Young's modulus of PZT patch, $\bar{E}_p = E_p(1+\eta \mathrm{i})$
f	frequency
G_a, G	shear rigidity of bonding layer and host beam, respectively
h_p, h_a, h_s	thickness of piezoelectric patch, bonding layers and host beam, respectively
i	$\sqrt{-1}$
I	moment of area
I_c	electric current
l	length of host structural member
l_p	length of PZT patch
M, Q	bending moment and shear force, respectively
t	time variable
T_1	longitudinal stress in PZT patch
u_N	axial displacement due to axial force in host structures
u_p	axial displacement
u_s	axial displacement on the surface of the host beam
V	electric voltage
w	transverse deflection
w_p	width of PZT patch
x, y, z	Cartesian coordinates
Y, Z	electric admittance and impedance of PZT patch, respectively
Z_s	mechanical impedance of the beam
Γ	shear lag parameter $\Gamma = \sqrt{(\bar{G}\theta_a/\bar{h}_a^2)(\psi+\alpha)/\psi}$, where $\bar{G} = G_a/E_p$, $\theta_a = h_a/h_p$, $\bar{h}_a = h_a/a$, $\alpha = 1$
δ	dielectric loss factors
$\varepsilon_{33}^{\mathrm{T}}$, $\bar{\varepsilon}_{33}^{\mathrm{T}}$	dielectric constant and complex dielectric constant, respectively $\bar{\varepsilon}_{33}^{\mathrm{T}} = \varepsilon_{33}^{\mathrm{T}}(1-\delta \mathrm{i})$
ε_p	axial strain of PZT patch
η	mechanical loss factors
κ	shear correction factor ($\pi^2/12$)
μ	Poisson's ratio of host structural member
ρ_p, ρ_s	mass density of PZT patch and host structures, respectively
$\tau(x)$	transferred shear stress between PZT patch and the host beam
φ	shear rotation
ψ	stiffness ratio, $\psi = E_s h_s/(E_p h_p)$
ω	circular frequency

integrity at high-frequency, as has been validated by many experimental investigations [4,8–12]. These vibration-based techniques have another limitation that the low-frequency measurement data is more prone to contamination by ambient vibrational noise and it happens in the low-frequency range [12]. On the other hand, the high-frequency EMI signature is usually isolated from the normal operating low-frequency vibrations, for instance when a truck crosses a bridge [9].

In contrast to extensive experimental study using the EMI technique, limited theoretical work on its modeling has been reported due to complexity of structures and difficulty in high-frequency analysis [13,14]. In fact, to date this technique has been unable to correlate changes in the signature to physical parameters of structures. Liang et al. [15], Zhou et al. [16] and Zagrai and Giurgiutiu [14,17] formulated analytical solutions based on EMI spectrum and mechanical response of a simple structure. When damages are induced in structures resulting in possible inhomogeneity of material properties, it is nonetheless very difficult to extend their formulation directly especially for interpreting the nature of damages. In the high-frequency range, approximate approaches such as the finite-element method (FEM) [7,18–24], spectral element method [25] and Ritz method [26,27] have been employed to quantitatively identify structural damages. However, various analytical difficulties do still exist. For example, FEM is usually subjected to an inherent disadvantage of low efficiency in high-frequency analysis of structure because it involves huge number of degree of freedom that requires huge number of finite elements and nodes for predicting sufficiently accurate results. Recently, Lim et al. [27,28] developed a DSC-Ritz method for high-frequency vibration analysis in which very accurate solutions for frequencies as high as the thousandth modes can be obtained numerically. But, they only considered isotropic materials without composite layers.

A mixed analysis integrated with transfer matrix method (TMM) and joint coupling matrices (JCM) was proposed by Nagem and Williams [1] who claimed the method very effective and accurate for dynamic analysis of a framed structure. However, it still suffers from numerical instability and insufficient accuracy in the high-frequency range especially for a structure containing some thin slender structural members as the conventional TMM does [1,29]. This will be discussed in Section 5 in an example. Recently, a reverberation matrix method (RMM) was first proposed by Pao et al. [2,3] to study the transient response of a plane truss consisted of elastic members. This method can be employed to overcome the difficulty associated with high-frequency analysis. It is extended here to investigate dynamics of a smart structure system.

The strain/stress transfer between PZT patches and host structures is physically implemented through bonding adhesives. In order to develop a more accurate model to improve sensitivity of impedance signature to damages in structure, the property of bonding layers should be considered. Furthermore, the inertia effect of actuator also should be taken into account because EMI technique employs high-frequency electric field with typical propagation wave length comparable to the length of actuator [30].

In this paper, a single PZT patch with free ends bonded onto a member of a framed structure is assumed in a state of pure one-dimensional (1D) axial vibration [14,15] under a harmonic electric excitation. A shear lag model [31,32] is employed to describe the properties of bonding layer. The structural members are modeled as Timoshenko beams for flexural vibration and as classical longitudinal rods for axial vibration. Damage is modeled as a reduction of Young's modulus in the member [26,33]. A coupled approach combining the EMI technique with RMM is proposed to relate the EMI signature with dynamics of the coupled structure system. It is shown that EMI signature can be extracted at least theoretically to identify damages in the framed structures.

2. Analytical formulation of structural members

As shown in Fig. 1, a planar framed structure consists of many 1D members are connected by rigid joints. The joints are assumed to be massless and the members are modeled as Timoshenko beams for flexural vibration and as classical longitudinal rods for axial vibration. A piezoelectric patch is bonded on the surface of an identified member as a sensor/actuator to detect structural damages. For a single structural member without bonded PZT patch, the assumption of small deflection is adopted, and hence, flexural deformation and axial deformation are uncoupled. Thus, the following relations hold:

$$\frac{\partial M}{\partial x} - Q + \rho_s I \frac{\partial^2 \varphi}{\partial t^2} = 0, \quad M = -E_s I \frac{\partial \varphi}{\partial x}, \quad \frac{\partial Q}{\partial x} = \rho_s A \frac{\partial^2 w}{\partial t^2}, \quad Q = \kappa A G \left(\frac{\partial w}{\partial x} - \varphi \right),$$
$$\frac{\partial N}{\partial x} = \rho_s A \frac{\partial^2 u_N}{\partial t^2}, \quad N = E_s A \frac{\partial u_N}{\partial x}, \tag{1}$$

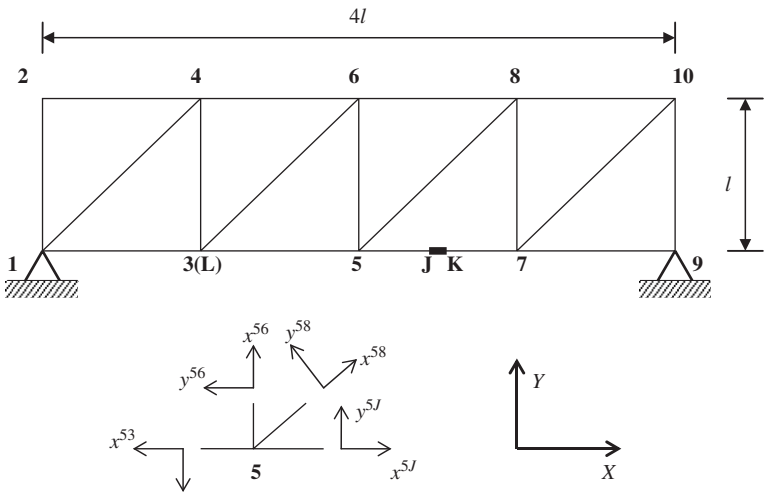

Fig. 1. A planar frame with one member bonded with a PZT patch and local coordinates.

where some terms in the equations above are of reverse sign with respect to some texts due to different sign convention. The steady-state solution under harmonic force can be written as

$$\begin{aligned} w(x,t) &= \left(a_2\,\mathrm{e}^{k_1 x} + a_3\,\mathrm{e}^{k_2 x} + d_2\,\mathrm{e}^{-k_1 x} + d_3\,\mathrm{e}^{-k_2 x}\right)\mathrm{e}^{\mathrm{i}\omega t},\\ \varphi(x,t) &= \left(\gamma_{s1}a_2\,\mathrm{e}^{k_1 x} + \gamma_{s2}a_3\,\mathrm{e}^{k_2 x} - \gamma_{s1}d_2\,\mathrm{e}^{-k_1 x} - \gamma_{s2}d_3\,\mathrm{e}^{-k_2 x}\right)\mathrm{e}^{\mathrm{i}\omega t},\\ u_N &= \left(a_1\,\mathrm{e}^{\mathrm{i}k_s x} + d_1\,\mathrm{e}^{-\mathrm{i}k_s x}\right)\mathrm{e}^{\mathrm{i}\omega t}, \end{aligned} \tag{2}$$

in which

$$k_1 = \begin{cases} \sqrt{\dfrac{-\left(\dfrac{\omega^2}{\kappa c_s^2}+\dfrac{\omega^2}{c_0^2}\right)+\sqrt{\left(\dfrac{\omega^2}{\kappa c_s^2}-\dfrac{\omega^2}{c_0^2}\right)^2+\dfrac{4\omega^2}{c_0^2 r_s^2}}}{2}} & \text{if } \omega < \sqrt{\kappa}c_s/r_s,\\ \sqrt{\dfrac{\left(\dfrac{\omega^2}{\kappa c_s^2}+\dfrac{\omega^2}{c_0^2}\right)-\sqrt{\left(\dfrac{\omega^2}{\kappa c_s^2}-\dfrac{\omega^2}{c_0^2}\right)^2+\dfrac{4\omega^2}{c_0^2 r_s^2}}}{2}}\,\mathrm{i} & \text{if } \omega > \sqrt{\kappa}c_s/r, \end{cases}$$

$$k_2 = \sqrt{\frac{\left(\dfrac{\omega^2}{\kappa c_s^2}+\dfrac{\omega^2}{c_0^2}\right)+\sqrt{\left(\dfrac{\omega^2}{\kappa c_s^2}-\dfrac{\omega^2}{c_0^2}\right)^2+\dfrac{4\omega^2}{c_0^2 r_s^2}}}{2}}\,\mathrm{i},$$

$$k_s^2 = \rho_s\omega^2/E_s, \quad \gamma_{si} = k_i + \frac{\omega^2}{\kappa c_s^2 k_i} \quad (i=1,2) \tag{3}$$

and a_i and d_i $(i=1,2,3)$ are undetermined constants. For a structural member with surface-bonded PZT wafer, a coupled system is considered, as shown in Fig. 2. The PZT patch is assumed in a state of 1D axial strain and the bonding layer is in a state of pure shear based on the shear lag model [31,32]. Hence, we have the following relations:

$$\text{PZT patch}: E_p\frac{\partial^2 u_p}{\partial x^2} - \frac{\tau(x)}{h_p} = \rho_p\frac{\partial^2 u_p}{\partial t^2},$$

$$\text{Bonding layer}: \tau = \frac{G_a}{h_a}(u_p - u_s), \quad u_s = u_N - \frac{h_s}{2}\frac{\partial w}{\partial x},$$

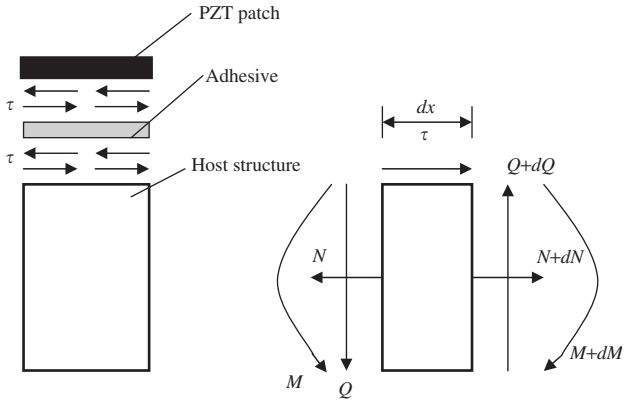

Fig. 2. A structural member with surface-bonded PZT wafer.

Host structural member:

$$\frac{\partial M}{\partial x}+\tau(x)h_s/2-Q+\rho_s I\frac{\partial^2\varphi}{\partial t^2}=0,\quad M=-E_sI\frac{\partial\varphi}{\partial x},\quad \frac{\partial Q}{\partial x}=\rho_sA\frac{\partial^2 w}{\partial t^2},$$
$$Q=\kappa AG\left(\frac{\partial w}{\partial x}-\varphi\right),\quad \frac{\partial N}{\partial x}+\tau(x)=\rho_sA\frac{\partial^2 u_N}{\partial t^2},\quad N=E_sA\frac{\partial u_N}{\partial x}. \tag{4}$$

Defining $k_p^2=\rho_p\omega^2/E_p$, $k_G^2=\rho_s\omega^2/\kappa G$, $u_N=\bar{u}_N\,\mathrm{e}^{\mathrm{i}\omega t}$, $u_p=\bar{u}_p\,\mathrm{e}^{\mathrm{i}\omega t}$, $\varphi=\bar{\varphi}\,\mathrm{e}^{\mathrm{i}\omega t}$ and $w=\bar{w}\,\mathrm{e}^{\mathrm{i}\omega t}$ yields the following four differential equations:

$$\bar{u}_N=\left[1-\frac{(\psi+1)k_p^2}{\psi(\Gamma/a)^2}\right]\bar{u}_p+\frac{h_s}{2}\frac{\mathrm{d}\bar{w}}{\mathrm{d}x}-\frac{\psi+1}{\psi(\Gamma/a)^2}\frac{\mathrm{d}^2\bar{u}_p}{\mathrm{d}x^2},$$
$$\frac{\mathrm{d}\bar{\varphi}}{\mathrm{d}x}=\frac{\mathrm{d}^2\bar{w}}{\mathrm{d}x^2}+k_G^2\bar{w},\quad \frac{\mathrm{d}\bar{w}}{\mathrm{d}x}=\alpha_1\frac{\mathrm{d}^6\bar{u}_p}{\mathrm{d}x^6}+\alpha_2\frac{\mathrm{d}^4\bar{u}_p}{\mathrm{d}x^4}+\alpha_3\frac{\mathrm{d}^2\bar{u}_p}{\mathrm{d}x^2}+\alpha_4\bar{u}_p,$$
$$\frac{\mathrm{d}^8\bar{u}_p}{\mathrm{d}x^8}+A_1\frac{\mathrm{d}^6\bar{u}_p}{\mathrm{d}x^6}+A_2\frac{\mathrm{d}^4\bar{u}_p}{\mathrm{d}x^4}+A_3\frac{\mathrm{d}^2\bar{u}_p}{\mathrm{d}x^2}+A_4\bar{u}_p=0, \tag{5}$$

where

$$\alpha_1=\frac{h_s}{6k_s^2}\frac{\psi+1}{\psi(\Gamma/a)^2},\quad \alpha_2=-\frac{2h_s}{3\psi k_s^2}-\frac{h_s}{6k_s^2}+\frac{h_s}{6k_s^2}(k_p^2+k_s^2+k_G^2)\frac{\psi+1}{\psi(\Gamma/a)^2},$$
$$\alpha_3=\frac{h_s}{k_s^2}\left[-\frac{2}{3\psi}k_p^2-\frac{k_s^2}{6}-\frac{k_G^2}{6}-\frac{k_G^2}{6\psi}+\left(\frac{k_G^2k_p^2}{6}+\frac{k_G^2k_s^2}{6}+\frac{k_s^2k_p^2}{6}\right)\frac{\psi+1}{\psi(\Gamma/a)^2}\right],$$
$$\alpha_4=-\frac{h_sk_G^2}{6k_s^2}\left[k_p^2/\psi+k_s^2-\frac{(\psi+1)k_s^2k_p^2}{\psi(\Gamma/a)^2}\right] \tag{6}$$

and

$$A_1=-\frac{4}{\psi+1}(\Gamma/a)^2-\frac{\psi}{\psi+1}(\Gamma/a)^2+k_p^2+k_G^2+2k_s^2,$$
$$A_2=k_s^4+2k_s^2k_p^2+2k_s^2k_G^2+k_G^2k_p^2-\frac{12k_s^2}{h_s^2}-(4k_s^2+4k_p^2+k_G^2)\frac{1}{\psi+1}(\Gamma/a)^2,$$
$$-(2k_s^2+k_G^2)\frac{\psi}{\psi+1}(\Gamma/a)^2,$$
$$A_3=-\left(k_G^2k_p^2+4k_s^2k_p^2+k_s^2k_G^2-\frac{12k_s^2}{h_s^2}\right)\frac{1}{\psi+1}(\Gamma/a)^2,$$
$$-\left(k_s^4+2k_s^2k_G^2-\frac{12k_s^2}{h_s^2}\right)\frac{\psi}{\psi+1}(\Gamma/a)^2+2k_G^2k_p^2k_s^2+k_s^4k_p^2+k_s^4k_G^2-\frac{12k_s^2}{h_s^2}k_p^2-\frac{12k_s^4}{h_s^2},$$
$$A_4=\left(k_s^2k_G^2-\frac{12k_s^2}{h_s^2}\right)\left(-k_p^2\frac{1}{\psi+1}(\Gamma/a)^2-k_s^2\frac{\psi}{\psi+1}(\Gamma/a)^2+k_s^2k_p^2\right). \tag{7}$$

From Eq. (5), we can obtain

$$u_p=\left(\mathbf{a}^{\mathrm{T}}\boldsymbol{\Omega}_a+\mathbf{d}^{\mathrm{T}}\boldsymbol{\Omega}_d\right)\mathrm{e}^{\mathrm{i}\omega t},$$
$$\varphi=\left(\mathbf{a}^{\mathrm{T}}\cdot\mathbf{diag}[\lambda_i]\cdot\boldsymbol{\Omega}_a+\mathbf{d}^{\mathrm{T}}\cdot\mathbf{diag}[\lambda_i]\cdot\boldsymbol{\Omega}_d\right)\mathrm{e}^{\mathrm{i}\omega t},$$
$$w=\left(\mathbf{a}^{\mathrm{T}}\cdot\mathbf{diag}\left[\gamma_i\right]\cdot\boldsymbol{\Omega}_a+\mathbf{d}^{\mathrm{T}}\cdot\mathbf{diag}\left[-\gamma_i\right]\cdot\boldsymbol{\Omega}_d\right)\mathrm{e}^{\mathrm{i}\omega t},$$
$$u_N=\left(\mathbf{a}^{\mathrm{T}}\cdot\mathbf{diag}\left[\eta_i\right]\cdot\boldsymbol{\Omega}_a+\mathbf{d}^{\mathrm{T}}\cdot\mathbf{diag}\left[\eta_i\right]\cdot\boldsymbol{\Omega}_d\right)\mathrm{e}^{\mathrm{i}\omega t}, \tag{8}$$

where

$$\mathbf{a} = \begin{bmatrix} a_1 & a_2 & a_3 & a_4 \end{bmatrix}^{\mathrm{T}}, \quad \mathbf{d} = \begin{bmatrix} d_1 & d_2 & d_3 & d_4 \end{bmatrix}^{\mathrm{T}},$$
$$\mathbf{\Omega}_a = \begin{bmatrix} \mathrm{e}^{\beta_1 x} & \mathrm{e}^{\beta_2 x} & \mathrm{e}^{\beta_3 x} & \mathrm{e}^{\beta_4 x} \end{bmatrix}^{\mathrm{T}}, \quad \mathbf{\Omega}_d = \begin{bmatrix} \mathrm{e}^{-\beta_1 x} & \mathrm{e}^{-\beta_2 x} & \mathrm{e}^{-\beta_3 x} & \mathrm{e}^{-\beta_4 x} \end{bmatrix}^{\mathrm{T}},$$
$$\gamma_i = \alpha_1 \beta_i^5 + \alpha_2 \beta_i^3 + \alpha_3 \beta_i + \alpha_4 / \beta_i, \quad \lambda_i = \gamma_i \beta_i + \gamma_i k_G^2 / \beta_i,$$
$$\eta_i = 1 - \frac{(\psi+1)k_p^2}{\psi(\Gamma/a)^2} - \frac{(\psi+1)}{\psi(\Gamma/a)^2}\beta_i^2 + \frac{h_s}{2}\gamma_i \beta_i \quad (i = 1, 2, 3, 4), \tag{9}$$

and **diag**[·] signifies a diagonal matrix, a_i and d_i $(i = 1, 2, 3, 4)$ are undetermined constants, and β_i are the characteristic roots of the fourth equation in Eq. (5). In RMM (to be discussed later), β_i should be arranged such that $\mathbf{a}^{\mathrm{T}}\mathbf{\Omega}_a$ corresponds to the arriving waves while $\mathbf{d}^{\mathrm{T}}\mathbf{\Omega}_d$ to the departing waves. This is particularly important to avoid numerical instability in the high-frequency range.

3. Dynamics of framed structures

In RMM, a major step is to set up two local coordinate systems for each homogeneous member as shown in Figs. 1 and 3. Having derived the transverse deflection, rotation and axial displacement for each member as in Eqs. (2) and (8), the bending moment, shear force and axial force can be obtained according to Eqs. (1) and (4). At a typical joint L, the balance of force and compatibility of motion must be considered. Thus, three equilibrium equations and $3(m^L-1)$ compatibility relations can be obtained (m^L is the number of members connected to joint L) which lead to the local scattering matrix of order $3m^L \times 3m^L$ at joint L. The detailed procedure is well established [2,3] for joints connected with elastic members and is omitted here for brevity. In the following, however, local scattering matrices at joints linked with smart members are derived as an illustrative example. As shown in Fig. 1, a single PZT patch is assumed to be bonded to the JK member and the following relations should be satisfied:

Compatibility conditions:

$$w^{J5} + w^{JK} = 0, \quad \varphi^{J5} = \varphi^{JK}, \quad u_N^{J5} + u_N^{JK} = 0.$$

Balance conditions:

$$M^{J5} + M^{JK} = 0, \quad Q^{J5} = Q^{JK}, \quad N^{J5} = N^{JK},$$
$$\text{at} \quad x^{J5} = x^{JK} = 0.$$

Boundary conditions at the end of PZT patch [31]:

$$\varepsilon_p = \frac{\partial u_p}{\partial x} = \Lambda = d_{31} E_3 = d_{31} V / h_p, \ \text{at} \ x^{JK} = 0. \tag{10}$$

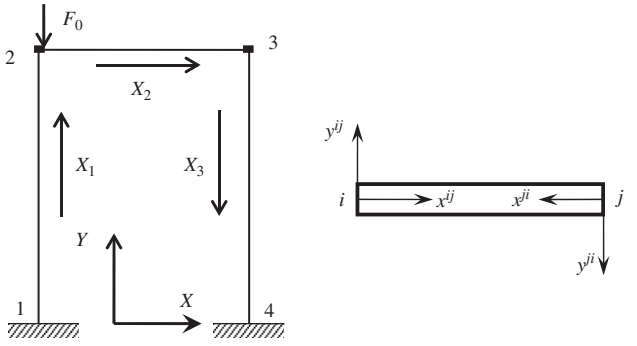

Fig. 3. A portal frame and local coordinates.

Substituting the expressions for all physical variables obtained from Eqs. (1), (2), (4) and (8) into Eq. (10) yield:

$$\mathbf{A}^J\mathbf{a}^J = \mathbf{B}^J\mathbf{d}^J + \mathbf{Q}_0, \tag{11}$$

where $\mathbf{A}^J$ and $\mathbf{B}^J$ can be readily derived from Eq. (10), and

$$\begin{aligned}
\mathbf{Q}_0 &= \begin{bmatrix} 0 & 0 & 0 & 0 & 0 & 0 & \Lambda \end{bmatrix}^{\mathrm{T}},\\
\mathbf{a}^J &= \begin{bmatrix} a_1^{J5} & a_2^{J5} & a_3^{J5} & a_1^{JK} & a_2^{JK} & a_3^{JK} & a_4^{JK} \end{bmatrix}^{\mathrm{T}},\\
\mathbf{d}^J &= \begin{bmatrix} d_1^{J5} & d_2^{J5} & d_3^{J5} & d_1^{JK} & d_2^{JK} & d_3^{JK} & d_4^{JK} \end{bmatrix}^{\mathrm{T}}.
\end{aligned}$$

Eq. (11) can be written as

$$\mathbf{d}^J = \mathbf{S}^J\mathbf{a}^J - (\mathbf{B}^J)^{-1}\mathbf{Q}_0, \tag{12}$$

where $\mathbf{S}^J = (\mathbf{B}^J)^{-1}\mathbf{A}^J$ is the local scattering matrix of order 7×7 at joint J. Denoting m and n the total numbers of structural members and joints in the frame, respectively, it is obvious that $\sum_{L=1}^{n} m^L = 2m$. Combining the $6m+2$ equations for all joints (the additional two equations are due to the boundary conditions at two ends of the piezoelectric patch), we arrive at a global scattering relation as follows:

$$\mathbf{d} = \mathbf{S}\mathbf{a} + \mathbf{Q}, \tag{13}$$

where $\mathbf{d} = [(\mathbf{d}^1)^{\mathrm{T}}, (\mathbf{d}^2)^{\mathrm{T}}, \ldots, (\mathbf{d}^{n-1})^{\mathrm{T}}, (\mathbf{d}^n)^{\mathrm{T}}]^{\mathrm{T}}$ is the global vector associated with departing waves, and $\mathbf{a} = [(\mathbf{a}^1)^{\mathrm{T}}, (\mathbf{a}^2)^{\mathrm{T}}, \ldots, (\mathbf{a}^{n-1})^{\mathrm{T}}, (\mathbf{a}^n)^{\mathrm{T}}]^{\mathrm{T}}$ is the global vector associated with arriving waves. The global scattering matrix is

$$\mathbf{S} = \begin{bmatrix}
\mathbf{S}^1_{6\times 6} & \cdots & \mathbf{0}_{6\times 7} & \mathbf{0}_{6\times 7} & \cdots & \mathbf{0}_{6\times 6}\\
\vdots & \ddots & \vdots & \vdots & \ddots & \vdots\\
\mathbf{0}_{7\times 6} & \cdots & \mathbf{S}^J_{7\times 7} & \mathbf{0}_{7\times 7} & \cdots & \mathbf{0}_{7\times 6}\\
\mathbf{0}_{7\times 6} & \cdots & \mathbf{0}_{7\times 7} & \mathbf{S}^K_{7\times 7} & \cdots & \mathbf{0}_{7\times 6}\\
\vdots & \ddots & \vdots & \vdots & \ddots & \vdots\\
\mathbf{0}_{6\times 6} & \cdots & \mathbf{0}_{6\times 7} & \mathbf{0}_{6\times 7} & \vdots & \mathbf{S}^n_{6\times 6}
\end{bmatrix} \tag{14}$$

and the global source vector is

$$\mathbf{Q} = \begin{bmatrix} (\mathbf{0}_{6\times 1})^{\mathrm{T}} & \cdots & [-(\mathbf{B}^J)^{-1}\mathbf{Q}_0]^{\mathrm{T}}_{7\times 1} & [-(\mathbf{B}^K)^{-1}\mathbf{Q}_0]^{\mathrm{T}}_{7\times 1} & \cdots & (\mathbf{0}_{6\times 1})^{\mathrm{T}} \end{bmatrix}^{\mathrm{T}}. \tag{15}$$

However, the $6m+2$ equations above are inadequate to solve for the total $12m+4$ unknowns in the two vectors $\mathbf{d}$ and $\mathbf{a}$. Thus, additional relations must be determined.

For each member, two different local coordinate systems have been employed. With a unique physical reality, solutions of the two systems should predict identical results. For example, at a certain point $x^{JK} = l^{JK} - x^{JK}$ of the member with bonded PZT patch, we have

$$u^{JK}(x^{JK}) = -u^{JK}(l^{JK} - x^{JK}) \tag{16}$$

which gives

$$a_1^{JK} = -d_1^{KJ}\,\mathrm{e}^{-\beta_1 l^{JK}}, \quad a_2^{JK} = -d_2^{KJ}\,\mathrm{e}^{-\beta_2 l^{JK}}, \quad a_3^{JK} = -d_3^{KJ}\,\mathrm{e}^{-\beta_3 l^{JK}}, \quad a_4^{JK} = -d_4^{KJ}\,\mathrm{e}^{-\beta_3 l^{JK}}. \tag{17}$$

The above equation can be written as

$$\mathbf{a}^{JK} = \mathbf{P}^{JK}\mathbf{d}^{KJ}, \tag{18}$$

where

$$\mathbf{P}^{JK} = \begin{bmatrix} -e^{-\beta_1 l^{JK}} & 0 & 0 & 0 \\ 0 & -e^{-\beta_2 l^{JK}} & 0 & 0 \\ 0 & 0 & -e^{-\beta_3 l^{JK}} & 0 \\ 0 & 0 & 0 & -e^{-\beta_4 l^{JK}} \end{bmatrix}. \tag{19}$$

Eqs. (17) and (18) present the relations connecting the arriving waves in one local coordinates to the departing waves in another local coordinates for a specific member and they are called the phase relations [2,3]. In order to avoid numerical instability as encountered in TMM, it should be emphasized that the phase relations should contain no exponential functions with large positive indices in the phase matrix $\mathbf{P}^{JK}$. This is a crucial point for proper application of RMM in dynamic analysis of structures.

Some new global vectors $\bar{\mathbf{d}}$ are introduced here, for example, $\bar{\mathbf{d}}$ at joint J can be expressed as follows:

$$\bar{\mathbf{d}}^J = \begin{bmatrix} d_1^{5J} & d_2^{5J} & d_3^{5J} & d_1^{KJ} & d_2^{KJ} & d_3^{KJ} & d_4^{KJ} \end{bmatrix}^{\mathrm{T}}. \tag{20}$$

The local vectors at all joints can be assembled to a single global matrix $\bar{\mathbf{d}}$ which contains the same elements as the vector $\mathbf{d}$ but sequenced in a different order. The two vectors thus can be related through a permutation matrix $\mathbf{U}$ as

$$\bar{\mathbf{d}} = \mathbf{U}\mathbf{d}, \tag{21}$$

where $\mathbf{U}$ is a $(6m+2) \times (6m+2)$ square matrix which contains one unit element in each row as well as one unit element in each column. Notice that the phase relations are valid for all structural members without and with PZT patches. Hence, these equations can be combined into a global phase shift relation as follows:

$$\mathbf{a} = \mathbf{P}\bar{\mathbf{d}}. \tag{22}$$

From Eqs. (13), (21) and (22), we obtain:

$$\mathbf{d} = \mathbf{R}\mathbf{d} + \mathbf{Q}, \quad \mathbf{R} = \mathbf{S}\mathbf{P}\mathbf{U}, \tag{23}$$

where $\mathbf{R}$ is called the reverberation ray matrix [2,3]. It is then obtained that:

$$\mathbf{d} = (\mathbf{I} - \mathbf{R})^{-1}\mathbf{Q}, \quad \mathbf{a} = \mathbf{S}^{-1}(\mathbf{d} - \mathbf{Q}) = \mathbf{S}^{-1}[(\mathbf{I} - \mathbf{R})^{-1} - \mathbf{I}]\mathbf{Q}. \tag{24}$$

Hence, all undetermined constants in Eqs. (2) and (8) can be solved for from Eq. (24).

4. Damage detection using EMI signature

In this section, we try to relate the EMI signature with dynamic characteristics of the coupled structure system analyzed here. As mentioned above, the PZT patch is considered as a thin bar undergoing only axial motion and is bonded to the JK member as shown in Fig. 1. Thus, the corresponding constitutive equations are [14,15,19,24]:

$$\varepsilon_p = \frac{T_1}{\bar{E}_p} + d_{31}E_3, \quad D_3 = \bar{\varepsilon}_{33}^{\mathrm{T}}E_3 + d_{31}T_1. \tag{25}$$

The electric current passing through PZT patch can be determined from the electric displacement as

$$I_c = \mathrm{i}\omega \iint D_3 \,\mathrm{d}x\,\mathrm{d}y = \mathrm{i}\omega w_p l_p \left(\bar{\varepsilon}_{33}^{\mathrm{T}} - d_{31}^2 \bar{E}_p\right) E_3 + \mathrm{i}\omega w_p d_{31} \bar{E}_p \left(u_p^{lp} - u_p^0\right), \tag{26}$$

where u_p^{lp} and u_p^0 represent the axial displacement on the right and left sides of PZT patch in the corresponding local coordinate, respectively. It is known that u_p is proportional to the electric voltage V according to Eqs. (10), (11), (15) and (24). Without loss of generality, a unit voltage is thus assumed. Substituting

the expression for u_p in Eq. (8) into Eq. (26) and then using the phase relations again yields the electric admittance as

$$Y = I_c/V = \mathrm{i}\omega w_p l_p\left(\bar{\varepsilon}_{33}^{\mathrm{T}} - d_{31}^2\bar{E}_p\right)/h_p + \mathrm{i}\omega w_p d_{31}\bar{E}_p\left(\sum_{j=1}^{4}(-a_j^{KJ} - a_j^{JK} - d_j^{JK} - d_j^{KJ})\right). \tag{27}$$

The electric impedance Z can be expressed as the inverse of electric admittance. From Eq. (27), the first term on right-hand side is only related to the PZT patch while the second term involves parameters of the PZT patch, the host member of the frame as well as the bonding layer. In fact, the second term indicates the resonance condition of coupled PZT patch–bond layer–host structure system in the frequency domain. If damage is induced, the EMI of the coupled structural system will change accordingly.

Many types of non-parametric indices such as root mean square deviation (RMSD), mean absolute percentage deviation (MAPD), covariance (Cov) and correlation coefficient (CC) have been employed to quantify changes in the EMI signature [34]. For example, the Cov index evaluates the averaged product of deviations of admittance signature data points from their respective means. Mathematically, it is defined as [34]

$$\mathrm{Cov} = \frac{1}{N}\sum_{i=1}^{N}(x_i - \bar{x})(y_i - \bar{y}), \tag{28}$$

where $\bar{x}$ and $\bar{y}$ are the mean values of two sets of admittance signature. Cov is a measure of the relationship between two signatures and it is used to determine whether two ranges of data move together. When the peak of one signature is in phase with the peak of the other signature, the Cov index is positive. On the contrary, the Cov is negative when the trough of one signature is in phase with the peak of the other. When both signatures are unrelated, the Cov is nearly zero. Thus damages can be characterized because the Cov is closer to zero or becomes negative for large deviation between signatures.

5. Numerical computation and discussion

Consider first a portal frame subjected to a harmonic mechanical force at joint 2 as shown in Fig. 3. The geometric parameters and material constants of the frame are listed in Table 1. The Euler–Bernoulli beam theory (EBT) and Timoshenko beam theory (TBT) for flexural vibration are adopted for comparison. The mixed analysis method referred as TMM–JCM [1] is also employed to investigate dynamics of this portal frame for comparison. The local coordinates X_1, X_2 and X_3 depicted in Fig. 3 are set up for this mixed analysis. We define the following quantity at joint 2 (Y direction):

$$Z_s = F_0/\dot{w}^{23}, \quad \dot{w}^{23} = \mathrm{d}w^{23}/\mathrm{d}t \tag{29}$$

which is known as the mechanical impedance, a mechanical counterpart of electric impedance. Z_s is employed to study dynamics of the portal frame. Under harmonic mechanical force, we have

$$Z_s = F_0/(\mathrm{i}\omega w^{23}). \tag{30}$$

Clearly, the transverse displacement of members 2–3, w^{23}, reflects the dynamic property of the structure and hence the mechanical impedance.

A comparison between EBT and TBT in Fig. 4 indicates a certain deviation of peaks between the two curves for frequency higher than 1.5 kHz. Because shear deformation is neglected in the EBT, the global stiffness of an Euler–Bernoulli beam is greater than that of a Timoshenko beam. Thus, the peaks of conductance (the real

Table 1
Material constants and geometric parameters of a host structural member

l (mm)	μ	h_s (mm)	E_s (N/m^2)	ρ_s (kg/m^3)	Damping ratio
200	0.3	10	20E + 10	7750	0.01

part of admittance) predicted by TBT shift leftwards as shown in Fig. 4(a). It is noted that excited shear vibration modes only can be captured by TBT. For example, in the frequency range of 30–50 kHz, six peaks can be found by TBT as compared to only five peaks predicted by EBT. Generally speaking, the result of EBT differs considerably from that of TBT as shown in Fig. 4(b). However, in the vicinity of 38 kHz the two curves can hardly be distinguished because this corresponds to a pure axial mode and in this analysis axial vibration is governed by an identical equation regardless of different beam bending theories.

Based on EBT, a comparison between RMM and TMM–JCM is conducted as shown in Fig. 5. It can be seen that the two methods agree with each other very well in the low-frequency range. However, when the frequency becomes higher, numerical instability appears in TMM–JCM while the method of RRM still behaves quite well. A recent work of the authors on a single Euler–Bernoulli beam indicated similar conclusion [35]. A similar comparison based on TBT is described in Fig. 6. It can be seen that the two curves can hardly be distinguished in the range of 1–10 kHz. However, for a portal frame with thin slender members ($l = 600$ mm while the other parameters are invariant), numerical inaccuracy can be observed in Fig. 6(b) for the method in Ref. [1]. RMM still performs well even in the high-frequency range for the structure with slender

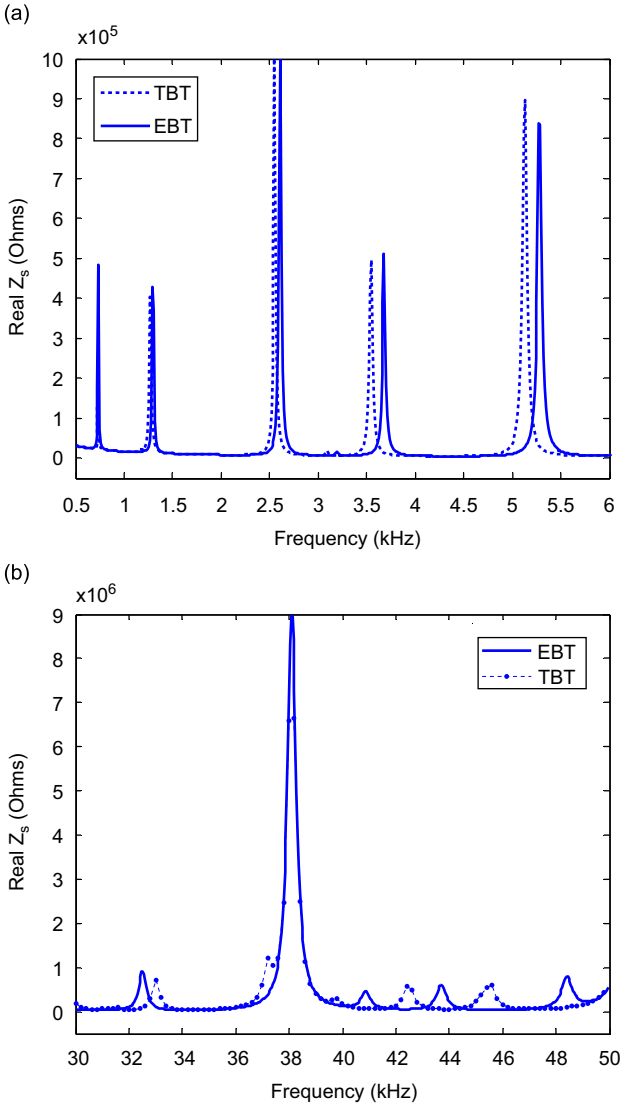

Fig. 4. Comparison between two beam theories.

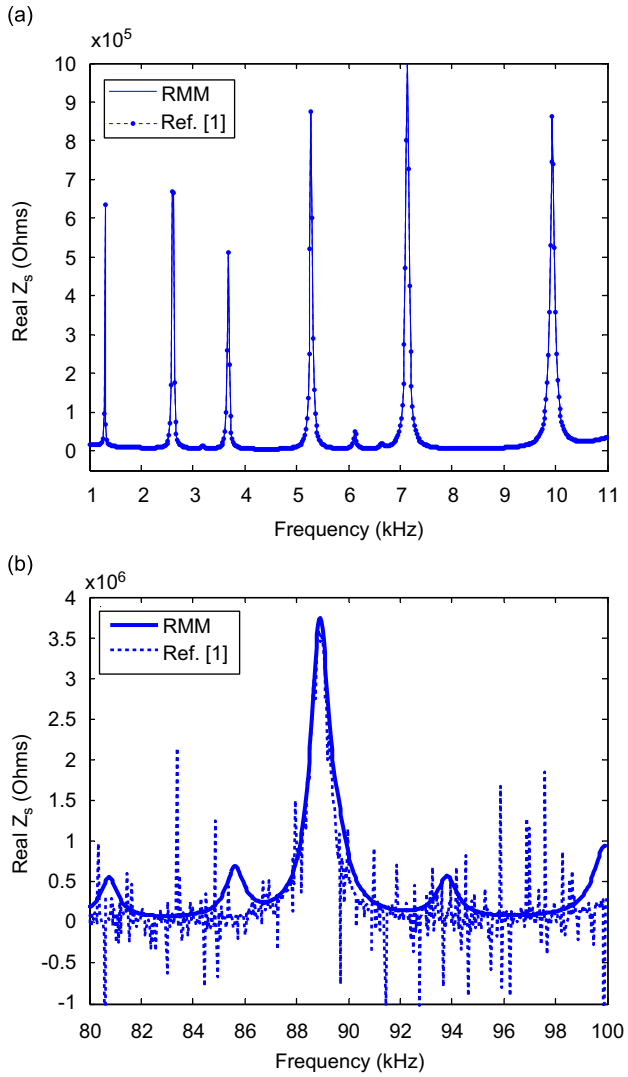

Fig. 5. Comparison with TMM–JCM based on EBT.

members. A close scrutiny in Figs. 5 and 6 finds an interesting phenomenon that numerical instability disappears in the vicinity of an axial mode frequency for which TMM–JCM agrees well with RMM. It is theoretically correct that TMM is able to deal with axial motion no matter how high the frequency is [36].

It is well known that measurement of mechanical impedance is very difficult for a structural system. On the other hand, it is rather easier to obtain electric impedance using a piezoelectric wafer. In this paper, a piezoelectric wafer is bonded onto the structural member and hence the electric impedance will vary with the dynamic property of host structure, as shown in Eq. (27). We next consider a more complicated framed structure where one member is surface-bonded with a PZT patch as shown in Fig. 1. The present coupled approach is now employed to relate the EMI signature with damage in the structural system. The geometric parameters and material constants of the elastic member and the PZT patch are listed in Tables 1 and 2, respectively. For convenience, we take the shear lag parameter $\Gamma = 129$ which assures an almost perfect bonding between the PZT patch and the member [31].

Three cases of damage corresponding to 40% reduction in Young's modulus of members 1–4, 3–6 and 5–8 are considered. They are referred to as P1, P2 and P3, respectively, and are used to study the effect of damage location on the EMI signature. It can be seen in Fig. 7 that the conductance (real part of the admittance)

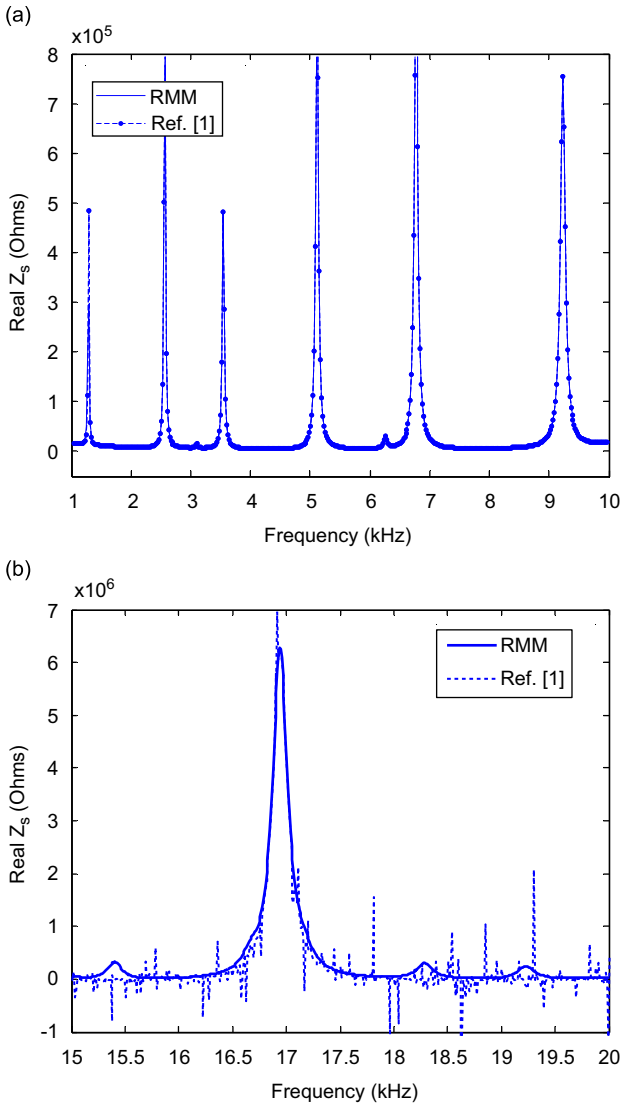

Fig. 6. Comparison with TMM–JCM based on TBT.

Table 2
Material constants and geometric parameters of PZT patch

Geometry (mm^3)	E_p (N/M^2)	η	ρ_p (kg/m^3)	d_{31} (m/V)	ε_{33}^{T} (F/m)	δ
$15 \times 10 \times 0.34$	6.67E+10	0.03	7800	−2.10E−10	2.14E−08	0.0185

spectrum for P1 can hardly be distinguished from the pristine one. However, the spectra for P2 and P3 are clearly different with P3 deviating significantly from the pristine one. The Cov shown in Fig. 8 predicts the same trend. Both figures indicate that the electro-mechanical signature measured from a PZT patch bonded onto a certain member is more sensitive to damages in the vicinity of the PZT patch which is in excellent agreement as reported [34].

In order to illustrate the sensitivity of EMI signature to the local incipient damage, we consider three cases of damage in 5-J segment with three severity degrees corresponding to 2%, 5% and 10% reduction in Young's

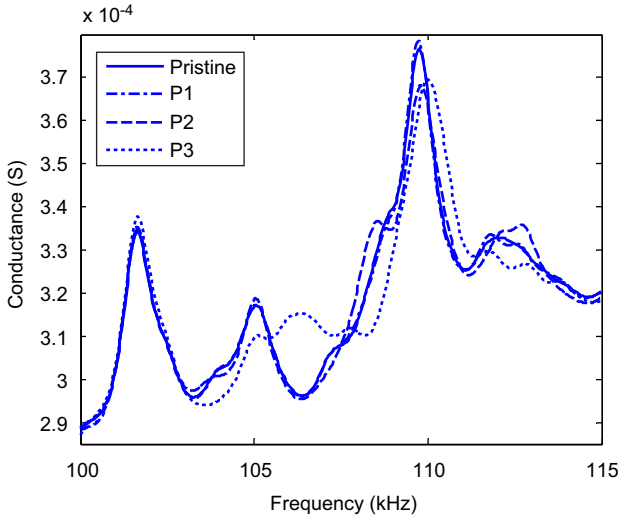

Fig. 7. EM admittance signature for various damage positions.

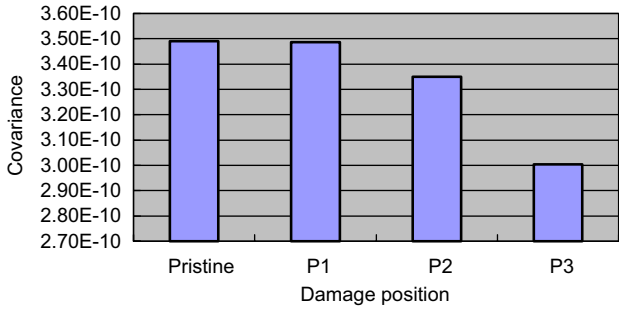

Fig. 8. Covariance versus damage position.

modulus (labeled as $D = 0.02$, 0.05 and 0.10, respectively). Fig. 9 shows the shift of resonant peaks towards the left with increasing damage severity due to reduction of global stiffness of host structure. Furthermore, new peaks can be observed between the dominant resonant frequencies for the case $D = 0.10$. These may correspond to certain secondary modes excited at high-frequency due to local damage. Meanwhile, the damage severity is also reflected clearly through Cov in Fig. 10.

To understand the effect of adhesive properties on the EMI signature, different shear lag parameters are now assumed. The shear lag parameter in Fig. 11, which directly reflects the bonding condition, has a significant effect on the conductance signature. Its effect even seems more significant than that of certain damage as shown by comparing with the P3 curve in Fig. 11. When bonding becomes weaker (i.e., decrease in shear lag parameter), the curve of conductance subsides down clearly. This agrees well with that observed by Bhalla and Soh [32]. However, it is interesting to note that no peak shift of conductance curve occurs for bonding imperfection in contrast with the obvious deviation of the P3 curve. This is mostly due to the fact that bonding conditions of a small PZT patch do not change significantly the global stiffness of structure although a coupled model is considered here. As a result, it can be concluded that even for significant changes EMI signature no peak shift of resonant frequencies occurs and the host structures may still be intact.

6. Conclusions

A new coupled approach combining RMM and EMI technique is proposed in this paper to identify analytically the local incipient damages in large framed structures. A shear lag model is adopted to depict the

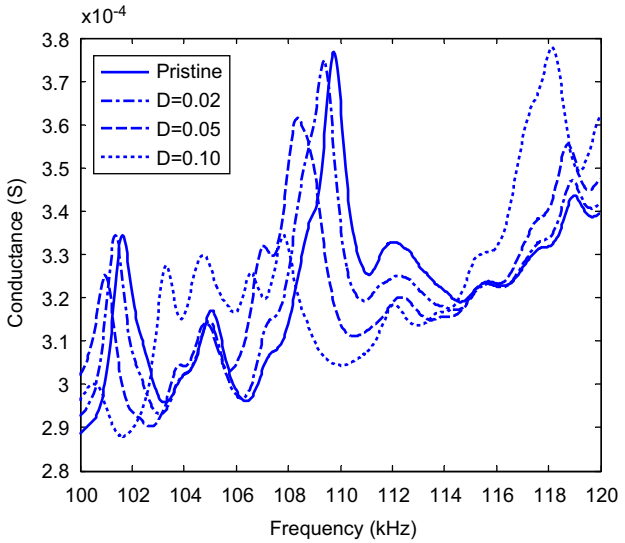

Fig. 9. EM admittance signature for different degrees of damage severity.

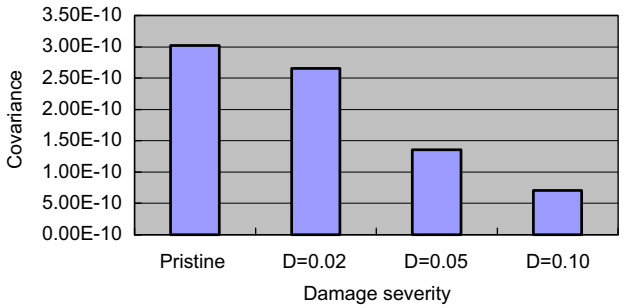

Fig. 10. Covariance versus damage severity.

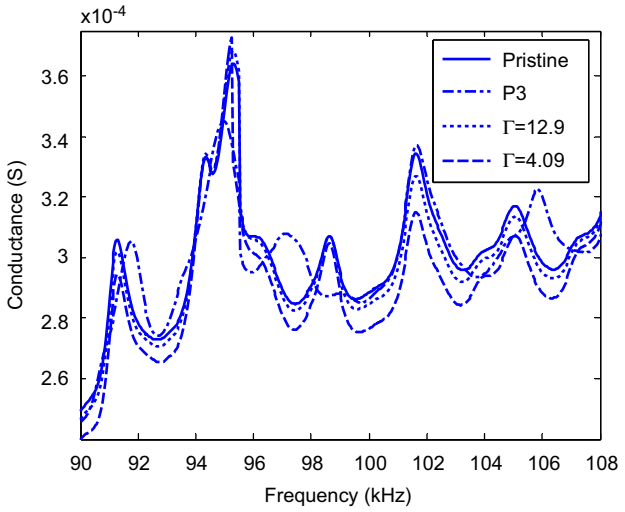

Fig. 11. Effect of imperfect bonding.

behavior of adhesives for considering the effect of interfacial conditions between PZT patches and the host member. The PZT wafer excited by high-frequency alternating electric field is assumed in 1D motion. The structural members are modeled as Timoshenko beams for flexural vibration and as classical longitudinal rods for axial vibration. An analytical expression for electric admittance is derived to quantitatively detect damages in a framed structure.

As predicted, the TBT is more appropriate to describe the high-frequency behavior of a beam as compared to the EBT [37]. A comparison study of mechanical impedance of a portal frame also confirms a significant difference between the two theories in high-frequency range. Comparison with TMM–JCM validates the precision and effectiveness of the analysis here. Numerical examples also indicate that the quantitative technique developed is able to correlate changes in signature to physical parameters of the host structure. Further information on severity and location of damages can also be provided. As it seems difficult to identify the severity and location of damages simultaneously and exactly by employing only a single PZT patch, an optimum study of distribution of multiple PZT patches will be carried out to solve this problem. This is however out of the scope of the current paper.

The effect of interfacial bonding behavior is also investigated. For imperfect bonding, the impedance signature changes accordingly which is, however, quite different from the peak deviation of conductance spectra induced by structural damages. This implies that even if a single PZT patch is imperfectly bonded onto the host structure in practice, the EMI signature thus obtained may still be valid and valuable for damage diagnosis through a proper analysis.

In summary, the new approach can be used to analyze dynamic response of a coupled model of PZT patch–bonding layer–host frame system even in the high-frequency range. Theoretically, it also provides an effective and convenient means to identify damage in the host structure. Although the analysis in this study is restricted to a planar frame, its extension to space frames is rather straightforward. Hence, the present approach is potentially a powerful tool for damage detection based on EMI.

Acknowledgements

This work was supported by the National Natural Science Foundation of China (No. 10432030) and by City University of Hong Kong (Project no. CityU 7001875 (BC)).

References

[1] R.J. Nagem, J.H. Williams, Dynamic analysis of large space structures using Transfer Matrices and Joint Coupling Matrices, *Mechanics of Structures and Machines* 17 (1989) 349–371.
[2] S.M. Howard, Y.H. Pao, Analysis and experiments on stress waves in planar trusses, *Journal of Engineering Mechanics* 124 (1998) 884–891.
[3] Y.H. Pao, D.C. Keh, S.M. Howard, Dynamic response and wave propagation in plane trusses and frames, *AIAA Journal* 37 (1999) 594–603.
[4] G. Park, H.H. Cudney, D.J. Inman, Feasibility of using impedance-based damage assessment for pipeline structures, *Earthquake Engineering and Structural dynamics* 30 (2001) 1463–1474.
[5] A. Alvandi, C. Cremona, Assessment of vibration-based damage identification techniques, *Journal of Sound and Vibration* 292 (2006) 179–202.
[6] C.K. Soh, K.K.H. Tseng, S. Bhalla, A. Gupta, Performance of smart piezoceramic patches in health monitoring of a RC bridge, *Smart Materials and Structures* 9 (2000) 533–542.
[7] A.S.K. Naidu, C.K. Soh, Damage severity and propagation characterization with admittance signatures of piezo transducers, *Smart Materials and Structures* 13 (2004) 393–403.
[8] F.P. Sun, Z. Chaudhry, C. Liang, C.A. Rogers, Truss structure integrity identification using PZT sensor–actuator, *Journal of Intelligent Material Systems and Structures* 6 (1995) 134–139.
[9] J.W. Ayres, F. Lalande, Z. Chaudhry, C.A. Rogers, Qualitative impedance-based health monitoring of civil infrastructures, *Smart Materials and Structures* 7 (1998) 599–605.
[10] G. Park, H.H. Cudney, D.J. Inman, Impedance-based health monitoring of civil structural components, *Journal of Infrastructure systems* 6 (2000) 153–160.
[11] G. Park, D.E. Muntges, D.J. Inman, Self-monitoring and self-healing jointed structures, *Key Engineering Materials* 204–205 (2001) 75–84.

[12] S. Bhalla, C.K. Soh, High frequency piezoelectric signatures for diagnosis of seismic/blast induced structural damages, *NDT & E International* 37 (2004) 23–33.
[13] G. Park, H.H. Cudney, D.J. Inman, An integrated health monitoring technique using structural impedance sensors, *Journal of Intelligent Material Systems and Structures* 11 (2000) 448–455.
[14] V. Giurgiutiu, A.N. Zagrai, Embedded self-sensing piezoelectric active sensors for on-line structural identification, *Journal of Vibration and Acoustics* 124 (2002) 116–125.
[15] C. Liang, F.P. Sun, C.A. Rogers, An impedance method for dynamic analysis of active material system, *Journal of Vibration and Acoustics* 116 (1994) 120–128.
[16] S.W. Zhou, C. Liang, C.A. Rogers, An impedance-based system modeling approach for induced strain actuator-driven structures, *Journal of Vibration and Acoustics* 118 (1996) 323–331.
[17] A.N. Zagrai, V. Giurgiutiu, Electro-mechanical impedance method for crack detection in thin plates, *Journal of Intelligent Material Systems and Structures* 12 (2002) 709–718.
[18] S. Bhalla, C.K. Soh, Z.X. Liu, Wave propagation approach for NDE using surface bonded piezoceramics, *NDT & E International* 38 (2005) 143–150.
[19] S. Bhalla, C.K. Soh, Structural healthing monitoring by piezo-impedance transducer, I: modeling, *Journal of Aerospace Engineering* 17 (2004) 154–165.
[20] S. Bhalla, C.K. Soh, Structural healthing monitoring by piezo-impedance transducer, II: applications, *Journal of Aerospace Engineering* 17 (2004) 166–175.
[21] Y.G. Xu, G.R. Liu, Modified electro-mechanical impedance model of piezoelectric actuator–sensor for debonding detection of composite patches, *Journal of Intelligent Material Systems and Structures* 13 (2002) 389–396.
[22] H.A. Winston, B.S. Annigeri, Structural health monitoring with piezoelectric active sensors, *Journal of Engineering for Gas Turbines and Power* 123 (2001) 353–358.
[23] A.S.K. Naidu, C.K. Soh, Identifying damage location with admittance signatures of smart piezo-transducers, *Journal of Intelligent Material Systems and Structures* 15 (2004) 627–642.
[24] K.K. Tseng, L.S. Wang, Impedance-based method for nondestructive damage identification, *Journal of Engineering Mechanics* 131 (2005) 58–64.
[25] S. Ritdumrongkul, M. Abe, Y. Fujino, T. Miyashita, Quantitative health monitoring of bolted joints using a piezoceramic actuator–sensor, *Smart Materials and Structures* 13 (2004) 20–29.
[26] J.F. Xu, Y. Yang, C.K. Soh, Electromechanical impedance-based structural health monitoring with evolutionary programming, *Journal of Aerospace Engineering* 17 (2004) 182–193.
[27] C.W. Lim, Z.R. Li, Y. Xiang, G.W. Wei, C.M. Wang, On the missing modes when using the exact frequency relationship between Kirchhoff and Mindlin plates, *Advances in Vibration Engineering* 4 (2005) 221–248.
[28] C.W. Lim, Z.R. Li, G.W. Wei, DSC-Ritz method for high-mode frequency analysis of thick shallow shells, *International Journal for Numerical Methods in Engineering* 62 (2005) 205–232.
[29] E.C. Pestel, F.A. Leckie, *Matrix Methods in Elasto Mechanics*, McGraw-Hill, New York, 1963.
[30] X.D. Wang, G.L. Huang, Wave propagation in electromechanical structures: induced by surface-bonded piezoelectric actuators, *Journal of Intelligent Material system and Structures* 12 (2001) 105–115.
[31] E.F. Crawley, J.D. Lius, Use of piezoelectric actuators as elements of intelligent structures, *AIAA Journal* 25 (1987) 1373–1385.
[32] S. Bhalla, C.K. Soh, Electromechanical impedance modeling for adhesively bonded piezo-transducers, *Journal of Intelligent Material Systems and Structures* 15 (2004) 955–972.
[33] U. Lee, J.A. Shin, Frequency-domain method of structural damage identification formulated from the dynamic stiffness equation of motion, *Journal of Sound and Vibration* 257 (2002) 615–634.
[34] K.K.H. Tseng, A.S.K. Naidu, Non-parametric damage detection and characterization using smart piezoceramic material, *Smart Materials and Structures* 11 (2002) 317–329.
[35] W. Yan, W.Q. Chen, J.B. Cai, C.W. Lim, Quantitative structural damage detection using high-frequency piezoelectric signatures via the reverberation matrix method, *International Journal for Numerical Methods in Engineering*, doi:10.1002/nme.1951 (4 December 2006).
[36] W. Yan, W.Q. Chen, C.W. Lim, J.B. Cai, Study on damage detection with high-frequency electric impedance signals, *Journal of Zhejiang University (Engineering Science)* 41 (2007) 6–11 (in Chinese).
[37] W.Q. Chen, C.F. Lu, Z.G. Bian, A semi-analytical method for free vibration of straight orthotropic beams with rectangular cross-sections, *Mechanics Research Communications* 31 (2004) 725–734.